Infrared spectra and band strengths of amorphous and crystalline N_2O

R. L. Hudson,[a] M. J. Loeffler, and P. A. Gerakines
Astrochemistry Laboratory, NASA Goddard Space Flight Center, Greenbelt, Maryland 20771, USA

(Received 27 September 2016; accepted 20 December 2016; published online 11 January 2017)

Infrared transmission spectra from 4000 to 400 cm^{-1}, and associated band strengths and absorption coefficients, are presented for the first time for both amorphous and crystalline N_2O. Changes in the spectra as a function of ice thickness and ice temperature are shown. New measurements of density, refractive index, and specific refraction are reported for amorphous and crystalline N_2O. Comparisons are made to published results, and the most-likely reason for some recent disagreements in the literature is discussed. As with CO_2, its isoelectronic congener, the formation of amorphous N_2O is found to require greater care than the formation of amorphous solids from more-polar molecules. [http://dx.doi.org/10.1063/1.4973548]

I. INTRODUCTION

Well-characterized molecular spectra play a central role in both laboratory astrochemistry and observational astronomy, and a healthy symbiosis exists between the two sources of data. Spectra acquired at ground-based and space-based observatories and those recorded by spacecraft can seldom be used to determine molecular abundances without input from laboratory measurements. Conversely, data on extraterrestrial objects can help drive Earth-bound research programs.

In our own laboratory, we have a well-established research program to determine the infrared (IR) spectra and reaction chemistry of known and suspected extraterrestrial molecules. Our studies have focused on molecules made from the four major biogenic elements (H, C, O, and N), and almost entirely at temperatures representative of objects from the orbit of Mars out to the edge of the solar system and into the interstellar medium. Past investigations by our group have included work on oxygen-hydrogen compounds (e.g., H_2O_2),[1] hydrocarbons (e.g., C_2H_2),[2] nitrogen-hydrogen molecules (e.g., NH_3),[3] carbon-nitrogen compounds (e.g., C_2N_2),[4] and carbon-oxygen compounds (e.g., CO).[5] The only two-element combination remaining from H, C, O, and N is nitrogen-oxygen, which we address in this paper.

At present the number of nitrogen-oxygen molecules identified by astronomers remains small. Among cometary molecules, only NO has been reported, in Comet Halley by Wallis and Krishna Swamy from uv-vis spectra.[6] An identification also has been made with radiowave methods[7] from the source Sgr B2, and recently Cernicharo *et al.* reported NO^+ toward the object Barnard 1-b.[8] The only other extraterrestrial nitrogen-oxygen molecule reported is N_2O, nitrous oxide, which was found by Ziurys *et al.* in the interstellar source Sgr B2(M),[9] and for which Jamieson *et al.* explored low-temperature synthetic pathways.[10]

Despite nitrous oxide's near-uniqueness among astronomical molecules, relatively little work has been done on the IR spectra of solid N_2O at temperatures representative of cold extraterrestrial environments. A very early study by Dows[11] established the major IR features and characteristics of solid N_2O, and later Yamada and Person[12] determined absolute intensities for the molecule's three fundamental vibrations for a crystalline sample at 65–80 K. Schettino and Salvi investigated two-phonon bands in crystalline N_2O at 77 K, assigning many new features.[13] Drobyshev and co-workers published a series of papers on IR spectra of solid N_2O and described how the gas-to-solid transition is accompanied by flashes of light (see the work of Drobyshev *et al.*[14] and references therein). A NASA technical report[15] contained two mid-IR survey spectra, but no enlargements to show details such as band shapes and widths. Ovchinnikov and Wight studied the inhomogeneous broadening of vibrational modes of several triatomic molecules, including N_2O, recording spectra of multiple features in both amorphous and crystalline samples.[16–18]

Among the more-recent work on solid N_2O is that of Fulvio *et al.*,[19] giving spectra of two fundamental and several overtone/combination bands for solid N_2O at 16 K, along with apparent band strengths for the ν_1 (1295 cm^{-1}), ν_3 (2239 cm^{-1}), and $2\nu_1$ (2581 cm^{-1}) features. Although these authors' experimental description contained many details, their spectra do not match those of Dows,[11] Yamada and Person,[12] Schettino and Salvi,[13] or Ovchinnikov and Wight,[16–18] and no reference was made to the phases of N_2O ices described by, among others, Drobyshev *et al.*[14]

In the present paper, we revisit the IR spectra of N_2O ices at 10–70 K, presenting new spectra of both the amorphous and crystalline phases along with IR band strengths. Since our experiments are motivated by possible astrochemical applications, and since the three N_2O fundamentals are the IR features most likely to be detected by astronomical observers, we focus on those three vibrations at the expense of the weaker overtone and combination bands. Finally, we also propose an explanation for the differences among some literature results.

[a] Author to whom correspondence should be addressed. Electronic mail: reggie.hudson@nasa.gov.

II. EXPERIMENTAL

Most of the procedures and equipment used were the same as described in recent papers from our laboratory, such as in the work of Moore *et al.*[4] and Hudson *et al.*[20] For spectral measurements, room temperature N_2O gas (Matheson) was leaked slowly into a vacuum chamber (10^{-8}–10^{-7} Torr) and condensed onto a pre-cooled KBr substrate (area ≈ 5 cm^2) at a rate that gave an increase in the sample's thickness of about 0.1–0.2 μm h^{-1}. Infrared transmission spectra were recorded with Thermo iS50 and Perkin Elmer Spectrum GX spectrometers from 4000 to 400 cm^{-1} with 100 scans per spectrum. Resolutions typically were 1 cm^{-1} for amorphous ices and 0.20 and 0.25 cm^{-1} for crystalline ones, with the IR beam aligned perpendicular to the plane of the ice sample. The use of two IR spectrometers, and occasionally an older Mattson Polaris instrument, was helpful for checking the reproducibility of the results. A blank, cooled KBr substrate was used as the background for all IR spectra reported here.

Each ice sample's thickness was measured by recording the interference fringes generated from light passing through the sample during the growth of ice. Under such conditions, the thickness is given by the equation

$$h = \frac{N_{fr}\lambda}{2\sqrt{n^2 - \sin^2\theta}} \quad (1)$$

from Ref. 21, where λ is the laser's wavelength (670 nm), n is the sample's refractive index at λ, N_{fr} is the number of interference fringes measured for the thickness h, and θ is the angle made by the laser's light perpendicular to the ice's surface. See the work of Hollenberg and Dows,[22] Groner *et al.*,[23] and Hudgins *et al.*[24] for additional information and our earlier papers for examples.

The values of n needed in Equation (1) initially were measured with the same two-laser interferometer that we have used in the past.[4] However, as our work progressed we also made measurements with a newly constructed two-laser interferometer (λ = 670 nm), with the incident laser beams at angles of θ_1 = 3.57 ± 0.04° and θ_2 = 53.57 ± 0.24° and the sample and substrate inside a new stainless-steel ultra-high vacuum (UHV) chamber (~10^{-10} Torr). Both our old and new sample chambers were interfaced with an infrared spectrometer with which the phase of each ice sample was determined. Although these two setups gave essentially the same values of n, our newer equipment had the advantage that the substrate was the gold surface of an INFICON quartz-crystal microbalance (QCM). This QCM, with a frequency resolution of about 0.1 Hz, was used to record data for calculating ice densities (ρ), which were needed to derive IR band strengths. These n and ρ measurements were similar to those of Satorre *et al.*[25] and Loeffler *et al.*[26] All of the n and ρ results in the present paper were obtained with our new UHV system.

III. RESULTS

A. Densities and refractive indices

Figure 1 is an example of our measurements of n and ρ. Panel (a) shows the interference patterns formed by our two laser beams reflecting from our gold substrate at angles of θ_1 and θ_2 while N_2O was being condensed on it at 70 K. Panel (b) of Figure 1 shows the corresponding frequency change of the QCM attached to our system, as measured at ~2-s intervals during this same N_2O deposition. The pronounced linearity of the data argues strongly for a constant deposition rate.

There are several ways in which the data of panels (a) and (b) of Figure 1 can be analyzed. For example, the fringe patterns in (a) can be fitted to an assumed mathematical form and the resulting fringe periods extracted.[27]

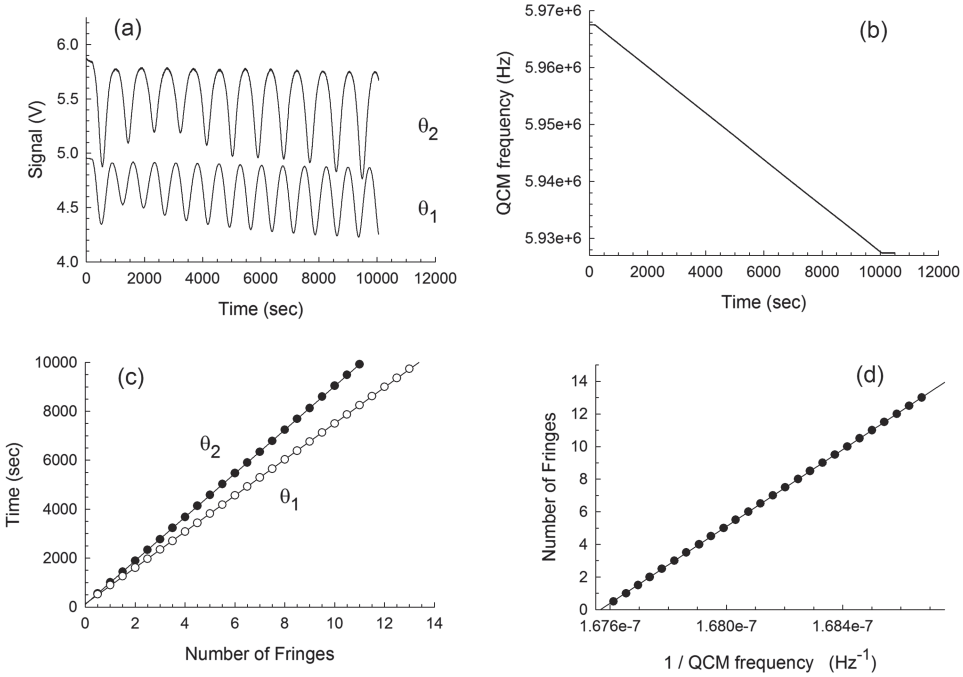

FIG. 1. Graphs to illustrate the procedure for determining n and ρ. The sample was N_2O deposited at 70 K. (a) Interference fringes recorded from two lasers during N_2O deposition, (b) frequency change in the quartz-crystal microbalance during N_2O deposition, (c) positions of the extrema of the two fringe patterns in (a), and (d) graph to determine the sample's density. See the text for details. In (b), the small flat regions just visible on the left and right are the QCM's steady, constant response before and after N_2O deposition, respectively.

However, we adopted a different approach that gave essentially the same results, and which is illustrated in Figure 1(c). The position (time) of each extremum in (a) was measured to an uncertainty of about 2 s for each of the two curves and then plotted as seen in panel (c). A linear least-squares fit is shown for the points from each fringe pattern, with the slopes of the two lines giving the periods t_1 and t_2 of the fringes. From this information, the equation

$$n = \sqrt{\frac{\sin^2\theta_2 - (t_1/t_2)^2\sin^2\theta_1}{1-(t_1/t_2)^2}} \quad (2)$$

gave n at 670 nm for N_2O. See also the paper of Tempelmeyer and Mills.[28]

There also are multiple ways to analyze the QCM data. The equation connecting ice density, ice thickness, and QCM frequency is

$$\rho = \frac{\kappa}{h}\left(\frac{1}{f} - \frac{1}{f_0}\right), \quad (3)$$

where f_0 is the initial frequency (at $h = 0$), f is the frequency at any later time, and $\kappa = 4.417 \times 10^5$ g Hz cm^{-2} (see the work of Lu and Lewis[29]). Substituting Equation (1) into Equation (3) and rearranging give

$$N_{fr} = \frac{2\kappa\sqrt{n^2 - \sin^2\theta}}{\lambda\rho}\left(\frac{1}{f}\right) - \frac{2\kappa\sqrt{n^2 - \sin^2\theta}}{\lambda\rho f_0}, \quad (4)$$

which has the form of an equation for a straight line. The implication is that a plot of the points (1/f, N_{fr}) for a set of fringes will have a slope given by

$$\frac{2\kappa\sqrt{n^2 - \sin^2\theta}}{\lambda\rho}, \quad (5)$$

from which ρ can be calculated. Panel (d) of Figure 1 shows such a plot for one N_2O deposition, where the points are taken at the same times as the θ_1 points in panel (c). All such graphs in our work had correlation coefficients greater than 0.9999.

Before proceeding, a comment on uncertainties in density is needed. Plots similar to panel (d) in Figure 1 were prepared using data from both our large- and small-angle lasers and gave the same ρ values. However, for our angles $\theta_1 = 3.57°$ and $\theta_2 = 53.57°$, the variation $(\partial\rho/\partial\theta_2)$ is nearly eight times greater than $(\partial\rho/\partial\theta_1)$, leading to much bigger overall uncertainties, u_ρ, in ice densities calculated from the large-angle laser. Further, when combined with the difference in uncertainties in the two lasers' positions (factor of six, ±0.04° vs. ±0.24°), u_ρ was over an order of magnitude bigger for the large-angle data than the small-angle data. In short, results obtained from both lasers gave the same ρ values, but since the small-angle laser gave much lower uncertainties (u_ρ) it was the only laser used to determine densities. These differences in uncertainties for the two lasers are inherent to the values of θ_1 and θ_2 selected and the form of Equation (5) for the slope in Figure 1(d).

Table I summarizes the accuracy and precision (reproducibility) of our n and ρ measurements on six N_2O ices. The uncertainties in accuracy, as represented by the standard errors listed for the twelve measurements, are from a propagation-of-error analysis.[30] For the precision, the largest variations are on the order of ±0.01 for n and ±0.01 g cm^{-3} for ρ, attesting to the high precision (low spread) of the data. Note that these uncertainties in precision are larger than those in accuracy. Strictly speaking, since the angle (position) of one of the lasers used for our measurements is known but to three significant figures, it is appropriate to round off the average values of n and ρ of Table I as follows: n(14 K) = 1.32, n(70 K) = 1.42, ρ(14 K) = 1.26 g cm^{-3}, and ρ(70 K) = 1.59 g cm^{-3}. Note, however, that in subsequent tables we often carry an additional significant figure for values of band intensities, which can again be rounded as desired.

TABLE I. Accuracy and precision of n and ρ for N_2O.[a,b]

Ice No.	Temperature, phase	n at 670 nm	Density (ρ, g cm^{-3})
1	14 K, amorphous	1.313 ± 0.004	1.256 ± 0.005
2	14 K, amorphous	1.324 ± 0.004	1.276 ± 0.005
3	14 K, amorphous	1.313 ± 0.004	1.256 ± 0.005
	Average =	1.317	1.263
	Standard error =	0.002	0.003
	Percent uncertainty =	0.175	0.229
	[b]Precision (standard deviation) =	0.006	0.012
4	70 K, crystalline	1.425 ± 0.004	1.594 ± 0.006
5	70 K, crystalline	1.421 ± 0.004	1.588 ± 0.006
6	70 K, crystalline	1.425 ± 0.004	1.592 ± 0.006
	Average =	1.424	1.591
	Standard error =	0.002	0.003
	Percent uncertainty =	0.140	0.218
	[b]Precision (standard deviation) =	0.002	0.003

[a]Accuracy refers to the uncertainty in each measurement of ρ and n as calculated with a propagation-of-error analysis. Standard error is defined as the uncertainty of the individual measurements divided by the square root of the number of determinations and percent uncertainty is 100 × (standard error/average).
[b]Precision refers to the variation (spread) in a set of measured values of ρ and n, here calculated as a standard deviation in the usual way.

B. Infrared spectra of N_2O—Fundamental vibrations

Figure 2 shows a typical survey spectrum of N_2O deposited at 10 K, with the three fundamental vibrations labeled. Although this spectrum conveys little information

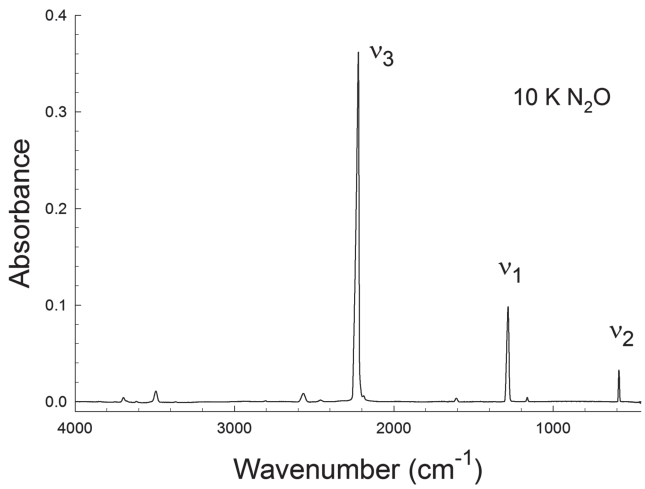

FIG. 2. A representative survey spectrum of amorphous N_2O at 10 K. The molecule's three fundamental vibrational bands are labeled. The sample's thickness was about 0.16 μm. See the text and tables for details concerning the weaker features.

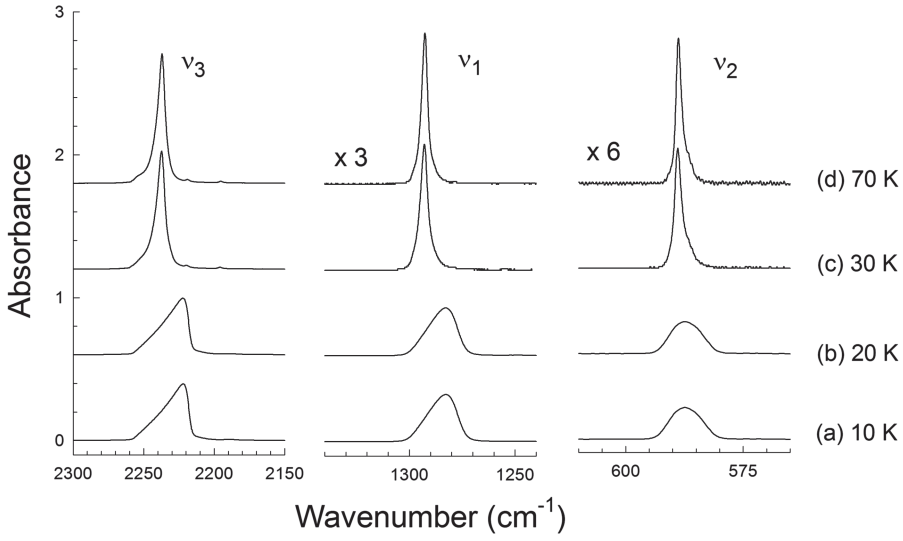

FIG. 3. Spectra of selected regions of N_2O deposited at 10 K and warmed to 70 K. The sample's thickness was about 0.18 μm. Note the vertical expansion factors of 3 and 6 for the ν_1 and ν_2 features, respectively, in (a)–(d). Spectra are offset vertically for clarity.

about specific IR shapes, it is useful for acquiring a quick appreciation of the low level of the noise, the relative intensities and the positions of various N_2O features, and the drift (little) in the baseline. Weak features near 3700, 2600, and 1600 cm^{-1} are from background H_2O in our vacuum system, which could be removed by extensive baking and pumping. Their presence or absence was not found to alter the final numerical results presented here. See our earlier paper on C_2H_2 for additional comments and another example.[2]

Figure 3 shows enlargements of the ν_1, ν_2, and ν_3 regions from Figure 2. Also shown is the result of warming the N_2O sample, with the significant changes at 20–30 K indicating a structural transition in the ice. Recooling the sample to 10 K did not regenerate the original spectrum. Solid N_2O (~1 μm thickness) was lost in about 10 min when warmed to 85 K in our vacuum system.

Anticipating our discussion (Section IV), the spectra for ices below 30 K and those at 30 K and above in Figure 3 are assigned to amorphous and crystalline N_2O, respectively. Table II lists positions and assignments for many of the more-prominent IR peaks of the amorphous and crystalline phases of N_2O at 10 K. All assignments were taken from the literature.[11,31–34]

Figure 4(a) shows the IR spectrum that resulted when N_2O gas was condensed at 70 K, but with all other conditions being the same as for Figures 2 and 3. Cooling the N_2O sample gave spectrum (b) of Figure 4. A comparison of these spectra for N_2O at (a) 70 K and (b) 10 K showed that peak positions did not change by more than a few tenths of a cm^{-1} and that band areas were constant to within about 1%. Spectrum (c) is that of an amorphous N_2O sample (made at 10 K) that was warmed to 70 K and then recooled to 10 K. The similarity of spectra (b) and (c) shows that direct deposition at a high temperature (i.e., 70 K) and crystallizing from the amorphous solid gave essentially the same crystalline N_2O ice on cooling to 10 K.

C. Infrared band intensities

Infrared spectra of N_2O were recorded as a function of the sample thickness for both the amorphous and crystalline phases to derive intrinsic spectral intensities in two ways. First, for the range of ice sizes used, the absorbance of a spectral peak was proportional to the ice sample's thickness, and since the optical depth is 2.303 × absorbance, then (2.303 × peak height) = $\alpha' h$, where α' is the peak's apparent absorption coefficient. This implies that a plot of optical depth for various ice thicknesses should be linear with a slope α', a measure of the band's intensity. The usual qualifications apply, such as concerning saturation and avoiding resolution-limited band shapes. A second measure of band strength derives from integration over an absorbance feature. Adopting the method of Hollenberg and Dows[22] and rearranging their equation give

$$2.303 \int_{band} (Absorbance)\, d\tilde{\nu} = (\rho_N A')h, \qquad (6)$$

TABLE II. Some IR features of solid N_2O at 10 K.[a]

Amorphous	Crystalline	Assignment
3492.8	3508.7	$\nu_1 + \nu_3$
3368.9	3380.1	$2\nu_2 + \nu_3$
2803.6	2814.3	$\nu_2 + \nu_3$
2567.3	2580.2	$2\nu_1$
2460.0	2468.8	$\nu_1 + 2\nu_2$
2221.5	2237.0	ν_3
...	2219.3	ν_3 ($^{15}N^{14}N^{16}O$)
2188.0	2195.6	ν_3 ($^{14}N^{15}N^{16}O$)
1882.0	1889.1	$\nu_1 + \nu_2$
1282.7	1292.9	ν_1
...	1278.7	ν_1 ($^{15}N^{14}N^{16}O$)
...	1255.1	ν_1 ($^{14}N^{14}N^{18}O$)
1162.6	1165.3	$2\nu_2$
587.7	589.0	ν_2
...	586.6	ν_2 ($^{15}N^{14}N^{16}O$)
...	585.7	ν_2 ($^{14}N^{14}N^{18}O$)

[a]Positions are in cm^{-1}; assignments are based on the work of Dows,[11] Giguère and Harvey,[31] LeRoy and Jouve,[32] Cahill and Ali,[33] and Łapiński *et al.*[34] with assignments of the weaker bands being more uncertain than those of the stronger ones.

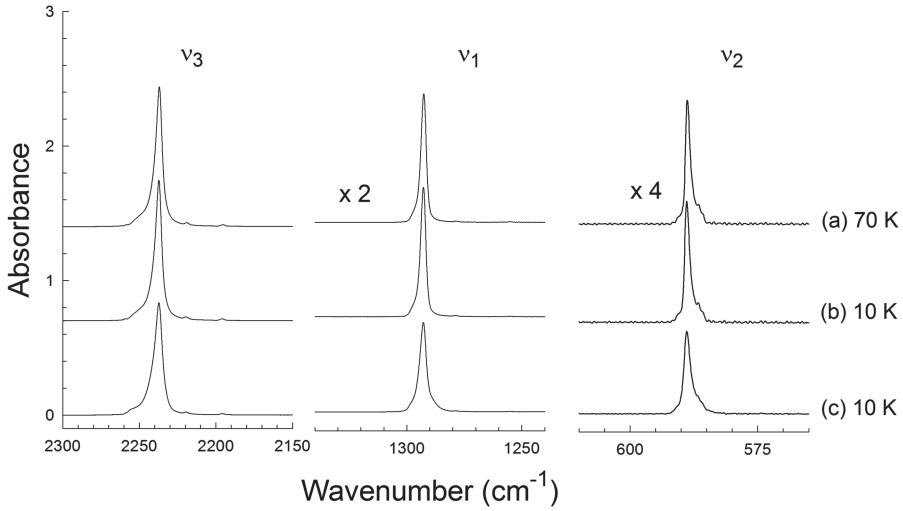

FIG. 4. Spectra of selected regions of crystalline N_2O ice (a) grown at 70 K and (b) cooled to 10 K compared to a sample that was (c) grown at 10 K, warmed to 70 K, and then recooled to 10 K. The ice's thickness was about 0.2 μm in each case. Note the vertical expansion factors of 2 and 4 for the ν_1 and ν_2 features, respectively, in (a)–(c). Spectra are offset vertically for clarity.

where ρ_N is the number density (molecules cm^{-3}) of N_2O molecules in the sample, h is again the sample's thickness, and $\tilde{\nu}$ is wavenumber in cm^{-1}. Equation (6) implies that a graph of the left-hand side as a function of the ice thickness (h) has a slope ($\rho_N A'$) from which the apparent band strength, A', can be calculated.

As examples, Figure 5 shows IR spectra of four amorphous-N_2O ices with different thicknesses. Figure 6 shows Beer's law type graphs of optical depth (=2.303 × absorbance peak height) and integrated optical depth (=2.303 × absorbance band area) as a function of the ice thickness. All six plots possess good linearity as $h \rightarrow 0$ so that apparent absorption coefficients (α') and apparent band strengths (A') could be calculated from their slopes.[2,35] Tables III and IV summarize band positions, widths, α' values, and A' values for N_2O deposited at 10 and 70 K. Results are included for all three fundamental vibrations.

D. Infrared spectra of N_2O—Other observations

During our work, several other observations were made that we wish to document. Features from a few N_2O isotopologues, such as $^{15}N^{14}N^{16}O$ and $^{14}N^{15}N^{16}O$, were seen in the spectra of Figures 2–4 but were not studied in any detail. Several such positions and assignments are given in Table II. Since the line widths of amorphous N_2O bands were larger than those of crystalline N_2O, isotopic features were easier to see in the latter.

As already stated, the ν_1, ν_2, and ν_3 vibrations of N_2O were the focus of our work. However, overtone and combination bands also were observed, and five such weak features in the spectrum of crystalline N_2O are labeled in the uppermost trace of Figure 7 with assignments taken from Dows.[11] The spectrum at the bottom of the same figure is that of amorphous N_2O. The middle spectrum of Figure 7 is that of an ice grown to give an increase in a thickness of about 0.2 μm h^{-1}, roughly twice the rate used for the bottom spectrum (amorphous N_2O). It is obvious from this figure that the middle spectrum is for an ice having both amorphous and crystalline components, showing that the solid phase formed at 10 K is sensitive to the rate at which N_2O is condensed from the gas phase.

Since we are unaware of band-strength measurements for any combination or overtone features of solid N_2O, in Tables V and VI we give intensity results for the molecule's $\nu_1 + \nu_3$, $2\nu_1$, and $2\nu_2$ absorbances for ice samples grown at 10 and 70 K. Intensities of other weak IR features of N_2O can be found by comparison to these three.

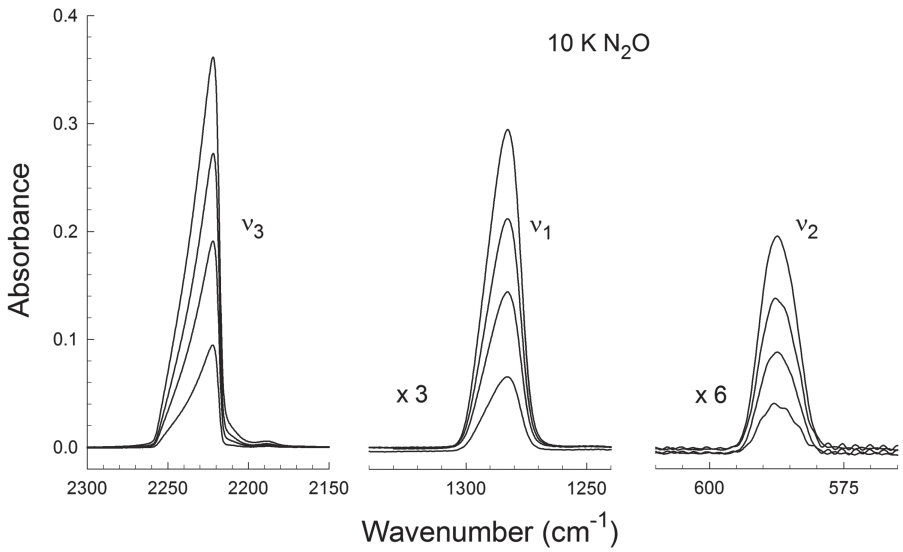

FIG. 5. Spectra for four amorphous ices at 10 K with thicknesses of about 0.04, 0.08, 0.12, and 0.16 μm. Note the vertical expansion factors of 3 and 6 for the ν_1 and ν_2 features, respectively.

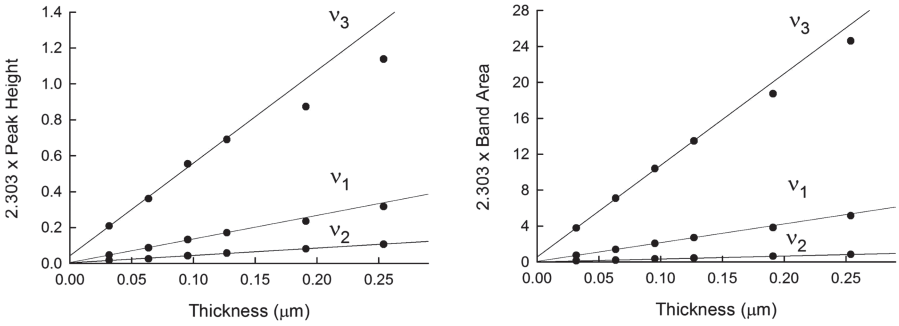

FIG. 6. Beer's law plots for the three fundamentals of amorphous N_2O at 10 K. For each vibration, the slope from its plot on the left is α', and $\rho A'$ for the plot on the right. For the lines associated with the ν_1 and ν_3 fundamentals, the points for the two thickest ices were ignored in computing the slope.

Previous workers demonstrated that the intensities of longitudinal optical (LO) components of a crystalline sample can be enhanced by a non-perpendicular alignment of the sample and the incident IR beam (e.g., Parker and Eggers;[36] Schettino and Salvi;[13] Cahill and Ali;[32] Ovchinnikov and Wight[16]). When our crystalline N_2O samples were rotated ~20° with respect to an axis perpendicular (normal) to the IR beam, the LO components of the ν_3, ν_1, and ν_2 bands appeared near 2258, 1299, and 591 cm^{-1}, respectively, supporting our description of the samples as crystalline. No such changes were observed in the samples we designated as amorphous. See the work of Cassidy *et al.*[37] for more, and in a different context, on the LO component and the issue of crystalline N_2O.

IV. DISCUSSION

A. Infrared spectra and N_2O phases

The linear, triatomic N_2O molecule belongs to the $C_{\infty v}$ point group and has 3N – 5 = 3(3) – 5 = 4 fundamental vibrations of which the ν_2 feature is doubly degenerate. Crystalline N_2O has T^4 ($P2_13$) symmetry with four molecules per unit cell.[38] A factor-group analysis, as summarized in Figure 8, leads to four IR-active transitions according to the usual selection rules (e.g., Anderson and Sun[39]). The two *F*-type transitions were not clearly resolved in our work. In Figure 4, about 2 cm^{-1} to the right of the large ν_2 large peak, is a shoulder that Schettino and Salvi assigned[13] to the second *F* component of crystalline N_2O. However, $\nu_2(^{15}N^{14}N^{16}O)$ should be at about the same position.[34]

As already stated, numerous weak overtone and combination bands were observed in our spectra. Positions of weak IR features of amorphous N_2O were not found in the literature, but our crystalline-N_2O features agreed with those published by others, such as by LeRoy and Jouve.[32] The strong features of (a) in Figure 4 agree with those reported by Yamada and Person for crystalline N_2O at 65–80 K.[12] Ovchinnikov and Wight investigated the broadening of the ν_3 band of N_2O deposited at 70 K, including the enhancement of the LO mode by a non-perpendicular alignment of the sample relative to the incident IR beam, an indicator of crystallinity.[16] Our results agree with those in both papers.

The N_2O spectrum of Figure 3(a) lacks the sharp substructure seen for the crystalline samples. Further, when the N_2O ice corresponding to this spectrum was warmed to 30 K, the spectrum changed irreversibly to that of crystalline N_2O. These observations led us to conclude that Figure 3(a) is for amorphous N_2O. Supporting this assignment is that in electron diffraction studies of solid N_2O, Krainyukova *et al.* observed[40] an amorphous-to-crystalline transition at 24–37 K, the same region as the transition between (b) and (c) in Figure 3. Finally, Ovchinnikov and Wight[16] published a spectrum of the ν_3 feature of N_2O from an ice made at 15 K. Their ice's spectrum was assigned to amorphous N_2O from the ν_3 peak being outside the limits of the LO and TO features at 2258 and 2237 cm^{-1}, respectively. The position and asymmetric shape of the ν_3 band in their amorphous N_2O sample's spectrum agree with our Figure 3(a), again supporting the latter's assignment to amorphous N_2O.

Osberg and Hornig[41] long ago identified measurements of ice thickness as a primary source of error in the type of work that we present here, an observation subsequently repeated by others (e.g., Refs. 24 and 42). In turn, the determination of ice thickness by interferometry, which we have used, depends on knowing or assuming the sample's refractive index at some wavelength. In addition, the conversion

TABLE III. IR fundamentals of amorphous N_2O at 10 K.[a]

Property	ν_3	ν_1	ν_2
$\tilde{\nu}$ /cm^{-1}	2 221.5	1 282.7	587.7
λ/μm	4.514 7	7.796 1	17.02
FWHM/cm^{-1}	20.2	16.2	7.7
α'/cm^{-1}	51 580 ± 2 372	13 120 ± 259	4 103 ± 111
$\rho_N A'$/cm^{-2}	1 018 000 ± 13 670	207 900 ± 1 684	26 270 ± 323
A'/cm $molecule^{-1}$	$5.891 \pm 0.079 \times 10^{-17}$	$1.203 \pm 0.010 \times 10^{-17}$	$1.520 \pm 0.019 \times 10^{-18}$
Integration range/cm^{-1}	2 265-2 200	1 310-1 260	592-584

[a]Sample made and spectrum recorded at 10 K; FWHM = full width at half maximum; α' and A' denote the apparent absorption coefficient and apparent band strength taken directly from a set of IR spectra using a Beer's law type plot, with $\rho_N = 1.728 \times 10^{22}$ molecule cm^{-3} (ρ = 1.263 g cm^{-3}; n = 1.317), as shown in Figure 6.

TABLE IV. IR fundamentals of crystalline N_2O at 70 K.[a]

Property	ν_3	ν_1	ν_2
$\tilde{\nu}$ /cm^{-1}	2 236.7	1 292.7	588.9
λ/μm	4.470 9	7.735 8	16.98
FWHM/cm^{-1}	5.1	2.7	1.1
α'/cm^{-1}	142 500 ± 9 002	57 310 ± 1 959	26 690 ± 641
$\rho_N A'$/cm^{-2}	1 111 000 ± 21 020	212 200 ± 5 163	40 580 ± 1 856
A'/cm molecule^{-1}	$5.103 \pm 0.097 \times 10^{-17}$	$9.747 \pm 0.237 \times 10^{-18}$	$1.864 \pm 0.085 \times 10^{-18}$
Integration range/cm^{-1}	2 265-2 221	1 304-1 280	592-584

[a]Sample made and spectrum recorded at 70 K; FWHM = full width at half maximum; α' and A' denote the apparent absorption coefficient and apparent band strength taken directly from a set of IR spectra using a Beer's law type plot with $\rho_N = 2.177 \times 10^{22}$ molecule cm^{-3} ($\rho = 1.591$ g cm^{-3}; $n = 1.424$), as shown in Figure 6.

of a spectral band area into a band strength (A') requires the sample's density. Here we have reported both n and ρ for two solid forms of N_2O at specific temperatures, but should more-accurate values of n and ρ appear then our results in Tables III–VI can easily be rescaled.

B. Comparisons to previous work

Yamada and Person[12] presented mid-IR spectra of crystalline N_2O near 77 K, and our band shapes and positions for N_2O at 70 K agree with theirs as well as with those of Dows[11] and Giguère and Harvey[31] at 80 and 98 K, respectively. Another earlier paper is the technical report of Roux *et al.*,[15] which has only a small amount of N_2O data and insufficient enlargements of spectra to show details. The authors' deposition temperature of 80 K would have generated crystalline N_2O, but the phase resulting from their 20 K deposition is difficult to know since the deposition rate, not just temperature, influences an ice's phase. In a paper by Sivaraman *et al.*,[43] N_2O had a peak absorbance of about 0.40 near 2240 cm^{-1} when deposited near 25 K for 90 s, a rate about 30 times faster than used for the present work. Not surprisingly, the resulting N_2O peak positions do not match those of our amorphous ice, but

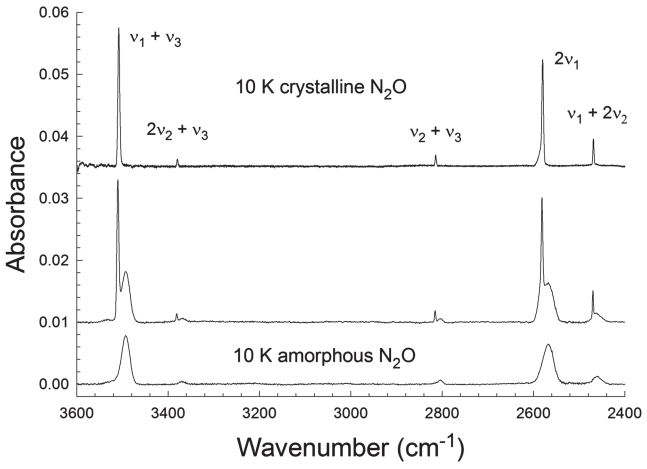

FIG. 7. Spectra of three N_2O ices at 10 K. Top: crystalline N_2O made at 70 K and cooled to 10 K; middle: two-phase N_2O ice; bottom: amorphous N_2O ice. Spectra are offset vertically for clarity. The thickness of the ice giving the top spectrum, and also of the ice giving the bottom spectrum, was about 0.13 μm, whereas the ice for the middle spectrum was slightly thicker. See the text for details.

rather they agree well with the positions for crystalline N_2O. (A sharp, unlabeled peak near 2260 cm^{-1} also suggests the crystallinity of the sample of Sivaraman *et al.*[43]) Finally, the single IR feature (ν_3) of amorphous N_2O shown by Ovchinnikov and Wight[16,18] agrees well with the shape of that same band in our Figures 3 and 5.

Comparisons to the recent N_2O study of Fulvio *et al.*[19] are straightforward. The ν_1 and ν_3 bands of their spectra of ices at 16 K possess shapes different from those in the IR spectra of our amorphous and crystalline N_2O samples. Also, the overtone and combination bands in their Figure 3 are essentially identical to those in the middle spectrum of our Figure 7 for an ice containing both amorphous and crystalline components. We conclude that their N_2O samples were mixtures of amorphous and crystalline ices. However, our Tables III and IV show that the integrated band strengths (A') of amorphous and crystalline N_2O are sufficiently close that measurements on an amorphous-crystalline N_2O mixture will fortuitously give A' values that are about the same as those from a purely amorphous (or crystalline) sample. The precise reasons for the partial crystallization of the samples of Fulvio *et al.*[19] are difficult to identify, but no N_2O condensation rate was stated by the authors. In our experience, for many small molecules, a high deposition rate, even with a substrate temperature near 10–20 K, can produce an ice that is wholly or partially crystalline.[2,34,44,45]

Turning from IR peak positions and band shapes, quantitative comparisons of our spectral intensities are more difficult. The only comparable work we have found is that of Yamada and Person[12] for crystalline N_2O, but substantial differences in equipment exist. Yamada and Person[12] used a dispersive IR spectrometer powered by vacuum-tube electronics and delivering analog data, whereas 52 years later we have employed Fourier-transform interferometer-based instruments delivering data in a digital form and based on a solid-state circuitry. Yamada and Person[12] reported that a different prism was used to study each of the three N_2O fundamentals, with resolving powers of 2–4 cm^{-1} whereas our resolution was 0.20–0.25 cm^{-1}. Perhaps as expected, the *relative* band strengths reported by Yamada and Person[12] for the three fundamentals of crystalline N_2O are close to ours, but those authors' *absolute* band strengths differ, being ~20% smaller than what we found. The specific reasons for this difference are unknown, but our much smaller resolution-to-linewidth ratio probably

TABLE V. IR overtone and combination bands of amorphous N_2O at 10 K.[a]

Property	$\nu_1 + \nu_3$	$2\nu_1$	$2\nu_2$
$\tilde{\nu}$ /cm^{-1}	3 492.8	2 567.3	1 162.6
λ/μm	2.863 0	3.895 1	8.601 4
FWHM/cm^{-1}	20.2	26.8	8.0
α'/cm^{-1}	1 479 ± 25.3	938.1 ± 11.1	549.1 ± 27.8
$\rho_N A'$/cm^{-2}	34 660 ± 682	26 270 ± 323	6 158 ± 215
A'/cm molecule^{-1}	$2.006 \pm 0.039 \times 10^{-18}$	$1.520 \pm 0.019 \times 10^{-18}$	$3.564 \pm 0.124 \times 10^{-19}$
Integration range/cm^{-1}	3 548-3 460	2 606-2 529	1 185-1 148

[a]Sample made and spectrum recorded at 10 K; FWHM = full width at half maximum; α' and A' denote the apparent absorption coefficient and apparent band strength taken directly from a set of IR spectra using a Beer's law type plot, with $\rho_N = 1.728 \times 10^{22}$ molecule cm^{-3} (ρ = 1.263 g cm^{-3}; n = 1.317), as shown in Figure 6.

is an important factor. Our n(70 K) and ρ(70 K) values for crystalline N_2O are similar to those in Yamada and Person,[12] so the problem indeed appears to be with differences in the spectral measurements.

As for amorphous N_2O, there are no reliable band strengths, and little other quantitative data beside peak positions, for comparison. Our n(14 K) is close to that of Roux *et al.*,[15] but the latter's ρ(20 K) = 0.988 g cm^{-3} seems much too small compared to expectations from liquid N_2O (1.22 g cm^{-3}, Ref. 46). Our density of 1.263 g cm^{-3} for amorphous N_2O is closer to the latter value.

Another way to compare our results to previous work is by calculating the specific refraction (r) of solid N_2O from

$$r = \frac{1}{\rho}\frac{n^2 - 1}{n^2 + 2}, \tag{7}$$

where n and ρ have the same meanings as before. Table I gives our n and ρ from which r = 0.1557 and 0.1604 cm^3 g^{-1} can be calculated for amorphous and crystalline N_2O, respectively. Again, comparison data are difficult to locate, but we found that Liveing and Dewar[47] measured n and ρ for liquid N_2O at its boiling point, 183 K. Their n(671 nm) = 1.338 and $\rho \approx 1.255$ g cm^{-3} give r = 0.1661 cm^3 g^{-1}. Yamada and Person[12] give r = 0.1570 cm^3 g^{-1} for crystalline N_2O (λ = 1100 nm). The average and standard error of these four values is 0.1598 ± 0.0023 cm^3 g^{-1} for a spread in r of 0.1575–0.1611 cm^3 g^{-1}. In contrast, the n and ρ of Roux *et al.*[15] yield r = 0.172 cm^3 g^{-1}, firmly outside this range. Their r is only about 7% higher than our average and it ignores any possible temperature influence. However, its use by Fulvio *et al.*[19] to calculate the density can explain, aside from uncertainties in the ice phase, why their $n(N_2O)$ appears to agree with one of our own, but their $\rho(N_2O)$ does not.

C. Comments on astrochemical applications

The icy solids found on comets, the surfaces of some solar system moons, and on interstellar grains are thought to be sufficiently cold that they will be amorphous, having never been warmed to their crystallization temperatures. However, our N_2O study again shows that the laboratory preparation of amorphous molecular solids is not always straightforward. Our work with C_2H_2, C_2H_4, CH_4, and CO_2, and the present study of N_2O, shows that condensation rates much lower than typically used for strongly and moderately polar compounds are sometimes needed to make amorphous samples of small molecules that are either non- or weakly polar. We found that a preparation of solid C_2H_2 at 10 K did not give the amorphous ice expected[48] but rather crystalline acetylene.[2] Similarly, an early IR study of C_2H_4 deposited at 4 K did not give an amorphous ice[49] but rather a metastable crystalline solid.[35] For CO_2 and CH_4, solid samples of each compound were prepared in multiple laboratories for over 20 years, and IR spectra published. We discovered that the reported spectra showed that these same CO_2 and CH_4 ices were either partially or fully crystalline, and not the amorphous solids assumed.[44,45] The cases of CO_2 and CH_4 ices were of particular importance given the significant interest in these solids by laboratory and observational astrochemists and the need for well-characterized IR spectra for large-scale space-based missions such as the James Webb Space Telescope.

In closing, we briefly suggest a few possible astrochemical uses of our work. First, the strongest IR band of N_2O is the ν_3

TABLE VI. IR overtone and combination bands of crystalline N_2O at 70 K.[a]

Property	$\nu_1 + \nu_3$	$2\nu_1$	$2\nu_2$
$\tilde{\nu}$ /cm^{-1}	3 507.7	2 579.8	1 165.2
λ/μm	2.850 9	3.876 3	8.582 2
FWHM/cm^{-1}	3.8	3.4	1.2
α'/cm^{-1}	9 759 ± 179	6 969 ± 146	3 918 ± 94
$\rho_N A'$/cm^{-2}	40 820 ± 978	30 950 ± 594	5 086 ± 142
A'/cm molecule^{-1}	$1.875 \pm 0.045 \times 10^{-18}$	$1.422 \pm 0.027 \times 10^{-18}$	$2.336 \pm 0.065 \times 10^{-19}$
Integration range/cm^{-1}	3 516-3 499	2 600-2 572	1 170-1 160

[a]Sample made and spectrum recorded at 70 K; FWHM = full width at half maximum; α' and A' denote the apparent absorption coefficient and apparent band strength taken directly from a set of IR spectra using a Beer's law type plot with $\rho_N = 2.177 \times 10^{22}$ molecule cm^{-3} (ρ = 1.591 g cm^{-3}; n = 1.424), as shown in Figure 6.

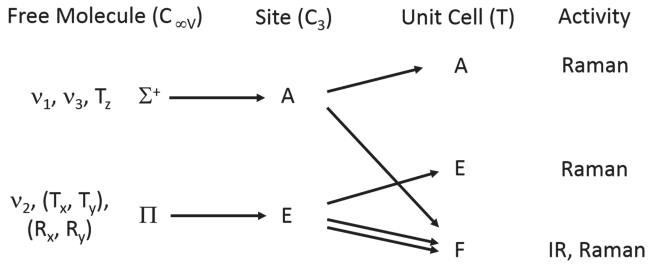

FIG. 8. Correlation diagram for N_2O showing vibrational transitions on going from the gas phase to the crystalline solid. The ν_1 and ν_3 vibrations each have an IR-active component, and the doubly degenerate ν_2 mode has two. Crystalline N_2O has four molecules per unit cell.

feature near 2230 cm^{-1}. Although we are unaware of any identifications of N_2O ice in that region by interstellar astronomers, our results can be used to set upper limits on N_2O abundances. Second, we have presented data only for the mid-IR spectral region. However, with care such data could be used to determine both near- and far-IR band intensities for N_2O. See the work of Sandford and Allamandola[50] and Giuliana *et al.*[51] for examples with other molecules. Third, our n(670 nm) values can serve as a starting point for Kramers-Kronig calculations of optical constants with which to determine α and A, the absolute absorption coefficients and band strengths of solid N_2O. Finally, our results are for one-component amorphous ices, but they can be considered as reasonable approximations for evaluating results in amorphous ice mixtures, such as $H_2O + N_2O$.

V. SUMMARY

We have presented for the first time mid-IR spectra and band strengths of both amorphous and crystalline N_2O, we have demonstrated the irreversible conversion of amorphous N_2O into crystalline N_2O, and we have shown spectra of N_2O ices as a function of the temperature and sample thickness. Extensive comparisons have been made to previous studies. New values of the density and refractive index are reported for amorphous and crystalline N_2O. Our work again emphasizes the close attention needed in the preparation of amorphous ices, particularly when the constituent molecules are non- or weakly polar.

ACKNOWLEDGMENTS

This work was supported by NASA's Astrophysics Research and Analysis program and assisted by a grant to the Goddard Center for Astrobiology from the NASA Astrobiology Institute.

[1]M. H. Moore and R. L. Hudson, Icarus **145**, 282 (2000).
[2]R. L. Hudson, R. F. Ferrante, and M. H. Moore, Icarus **228**, 276 (2014).
[3]M. H. Moore, R. F. Ferrante, R. L. Hudson, and J. N. Stone, Icarus **190**, 260 (2007).
[4]M. H. Moore, R. F. Ferrante, W. J. Moore, and R. L. Hudson, Astrophys. J. Suppl. Ser. **191**, 96 (2010).
[5]M. H. Moore and R. L. Hudson, Icarus **161**, 486 (2003).
[6]M. K. Wallis and K. S. Krishna Swamy, Astron. Astrophys. **187**, 329 (1987).
[7]H. S. Liszt and B. E. Turner, Astrophys. J. **224**, L73 (1978).
[8]J. Cernicharo, S. Bailleux, E. Alekseev, A. Fuente, E. Roueff, M. Gerin, B. Tercero, S. P. Treviño-Morales, N. Marcelino, R. Bachiller, and B. Lefloch, Astrophys. J. **795**, 1 (2014).
[9]L. M. Ziurys, A. J. Apponi, J. M. Hollis, and L. E. Snyder, Astrophys. J. **436**, L181 (1994).
[10]C. S. Jamieson, C. J. Bennett, A. Mebel, and R. I. Kaiser, Astrophys. J. **624**, 436 (2005).
[11]D. A. Dows, J. Chem. Phys. **26**, 745 (1957).
[12]H. Yamada and W. B. Person, J. Chem. Phys. **41**, 2478 (1964).
[13]V. Schettino and P. R. Salvi, Spectrochim. Acta, Part A **31**, 399 (1975).
[14]A. Drobyshev, A. Aldiyarov, E. Korshikov, V. Kurnosov, D. Sokolov, and N. Tokmoldin, Low Temp. Phys. **39**, 460 (2013).
[15]J. A. Roux, B. E. Wood, A. M. Smith, and R. R. Plyler, Arnold Engineering Development Center Report, AEDC-TR-79–81, 1980. Note that there is a 2% calculation error for $r(N_2O)$ in this paper.
[16]M. A. Ovchinnikov and C. A. Wight, J. Chem. Phys. **99**, 3374 (1993).
[17]M. A. Ovchinnikov and C. A. Wight, J. Chem. Phys. **100**, 972 (1994).
[18]M. A. Ovchinnikov and C. A. Wight, J. Chem. Phys. **102**, 67 (1995).
[19]D. Fulvio, B. Sivaraman, G. A. Baratta, M. E. Palumbo, and N. J. Mason, Spectrochim. Acta, Part A **72**, 1007 (2009).
[20]R. L. Hudson, P. A. Gerakines, and M. J. Loeffler, Phys. Chem. Chem. Phys. **17**, 12545 (2015).
[21]O. S. Heavens, *Optical Properties of Thin Solid Films*, 2nd ed. (Butterworths Scientific Publications and Dover, London and New York, 1955 and 2011), p. 114.
[22]J. Hollenberg and D. A. Dows, J. Chem. Phys. **34**, 1061 (1961).
[23]P. Groner, I. Stolkin, and H. H. Günthard, J. Phys. E: Sci. Instrum. **6**, 122 (1973).
[24]D. M. Hudgins, S. A. Sandford, L. J. Allamandola, and A. G. G. M. Tielens, Astrophys. J. Suppl. Ser. **86**, 713 (1993).
[25]M. Á. Satorre, M. Domingo, C. Millán, R. Luna, R. Vilaplana, and C. Santonja, Planet. Space Sci. **56**, 1748 (2008).
[26]M. J. Loeffler, M. H. Moore, and P. A. Gerakines, Astrophys. J. **827**, 98 (2016).
[27]C. Romanescu, J. Marschall, D. Kim, A. Khatiwada, and K. S. Kalogerakis, Icarus **205**, 695 (2010).
[28]K. E. Tempelmeyer and D. W. Mills, J. Appl. Phys. **39**, 2968 (1968).
[29]C. S. Lu and O. Lewis, J. Appl. Phys. **43**, 4385 (1972).
[30]J. R. Taylor, *An Introduction to Error Analysis* (University Science Books, Sausalito, California, 1997), pp. 45–79.
[31]P. A. Giguère and K. B. Harvey, Spectrochim. Acta **9**, 204 (1957).
[32]A. LeRoy and P. Jouve, Compt. Rend. **264B**, 1656 (1967).
[33]J. E. Cahill and N. Ali, Chem. Phys. Lett. **45**, 504 (1977).
[34]A. Łapiński, J. Spanget-Larsen, J. Waluk, and J. G. Radziszewski, J. Chem. Phys. **115**, 1757 (2001).
[35]R. L. Hudson, P. A. Gerakines, and M. H. Moore, Icarus **243**, 148 (2014).
[36]M. A. Parker and D. F. Eggers, Jr., J. Chem. Phys. **45**, 4354 (1966).
[37]A. Cassidy, M. R. V. Jørgensen, A. Rosu-Finsen, J. Lasne, J. H. Jørgensen, A. Glavic, V. Lauter, B. B. Iversen, M. R. S. McCoustra, and D. Field, J. Phys. Chem. C **120**, 24130 (2016).
[38]J. de Smedt and W. H. Keeson, Koninkl. Ned. Akad. Wetenschap. Proc. **27**, 839 (1924).
[39]A. Anderson and T. S. Sun, Chem. Phys. Lett. **8**, 537 (1971).
[40]N. V. Krainyukova, M. A. Strzhemechny, and A. S. Drobyshev, Fiz. Nizk. Temp. **22**, 455 (1996) [Low Temp. Phys. **22**, 123 (1996)].
[41]W. E. Osberg and D. F. Hornig, J. Chem. Phys. **20**, 1345 (1952).
[42]C. A. Poteet, K. M. Pontoppidan, S. T. Megeath, D. M. Watson, K. Isokoski, J. E. Bjorkman, P. D. Sheehan, and H. Linnartz, Astrophys. J. **766**, 1 (2013).
[43]B. Sivaraman, S. Ptasinska, S. Jheeta, and N. J. Mason, Chem. Phys. Lett. **460**, 108 (2008).
[44]P. A. Gerakines and R. L. Hudson, Astrophys. J. **805**, L20 (2015).
[45]P. A. Gerakines and R. L. Hudson, Astrophys. J. **808**, L40 (2015).
[46]A. J. Leadbetter, D. J. Taylor, and B. Vincent, Can. J. Chem. **42**, 2930 (1964).
[47]G. Liveing and J. Dewar, Philos. Mag. **34**, 205 (1892).
[48]N. Boudin, W. A. Schutte, and J. M. Greenberg, Astron. Astrophys. **331**, 749 (1998).
[49]M. W. Jacox, J. Chem. Phys. **36**, 140 (1962).
[50]S. A. Sandford and L. J. Allamandola, Astrophys, J. **417**, 815 (1993).
[51]B. M. Giuliana, R. M. Escribano, R. Martín-Doménech, E. Dartois, and G. M. Muñoz Caro, Astron. Astrophys. **565**, 108 (2014).